The evolved stars of Leo II dSph galaxy from near-infrared UKIRT/WFCAM observations

M. Gullieuszik[1][*], E. V. Held[1], L. Rizzi[2], L. Girardi[1], P. Marigo[3] and Y. Momany[1]

[1] *INAF/Osservatorio Astronomico di Padova, vicolo dell'Osservatorio 5, I-35122 Padova, Italy*
[2] *Joint Astronomy Centre, 660 N. A'ohoku Place, University Park, Hilo, HI 96720, USA*
[3] *Dipartimento di Astronomia, Università di Padova, vicolo dell'Osservatorio 2, I-35122 Padova, Italy*

ABSTRACT

We present a study of the evolved stellar populations in the dwarf spheroidal galaxy Leo II, based on JHK_s observations obtained with the near-infrared array WFCAM at the UKIRT telescope. Combining the new data with optical data, we derived photometric estimates of the distribution of global metallicity [M/H] of individual red giant stars from their $V - K_s$ colours. Our results are consistent with the metallicities of RGB stars obtained from Ca II triplet spectroscopy, once the age effects are considered. The photometric metallicity distribution function has a peak at [M/H] $= -1.74$ (uncorrected) or [M/H] $= -1.64 \pm 0.06$ (random) ± 0.17 (systematic) after correction for the mean age of Leo II stars (9 Gyr). The distribution is similar to a Gaussian with $\sigma_{\rm [M/H]} = 0.19$ dex, corrected for instrumental errors. We used the new data to derive the properties of a nearly complete sample of asymptotic giant branch (AGB) stars in Leo II. Using a near-infrared two-colour diagram, we were able to obtain a clean separation from Milky Way foreground stars and discriminate between carbon- and oxygen-rich AGB stars, which allowed to study their distribution in K_s-band luminosity and colour. We simulate the JHK_s data with the TRILEGAL population synthesis code together with the most updated thermally pulsing AGB models, and using the star formation histories derived from independent work based on deep HST photometry. After scaling the mass of Leo II models to the observed number of upper RGB stars, we find that present models predict too many O-rich TP-AGB stars of higher luminosity due to a likely under-estimation of either their mass-loss rates at low metallicity, and/or their degree of obscuration by circumstellar dust. On the other hand, the TP-AGB models are able to reproduce the observed number and luminosities of carbon stars satisfactorily well, indicating that in this galaxy the least massive stars that became carbon stars should have masses as low as $\sim 1 \, M_\odot$.

Key words: Galaxies: individual: Leo II – Galaxies: stellar content – stars: AGB and post-AGB – stars: carbon – Local Group

1 INTRODUCTION

Leo II is one of the most distant dwarf spheroidal (dSph) satellites of the Milky Way. A number of photometric studies derived quite different distances for Leo II. Mighell & Rich (1996), using the V magnitude of the horizontal branch (HB), placed the galaxy at a distance modulus $(m - M)_0 = 21.55 \pm 0.18$. Using the I band magnitude of the tip of the RGB (TRGB), Bellazzini, Gennari & Ferraro (2005) found $(m - M)_0 = 21.84 \pm 0.13$. Distance estimates in the literature are intermediate between these values, with typical uncertainties of ~ 0.2 magnitudes.

The estimates of mean metallicity of Leo II range from [Fe/H] $= -1.6$ (Mighell & Rich 1996) up to [Fe/H] $\simeq -1.1$ (Dolphin 2002). Recently, two independent spectroscopic studies, based on the Ca II triplet method, found Leo II to be relatively metal-poor: a mean value of [Fe/H] $= -1.74$ was derived by Koch et al. (2007) while Bosler, Smecker-Hane & Stetson (2007) found [Fe/H] $= -1.59$.

The Leo II dSph was considered for a long time as a typical "old" dSph. Then Mighell & Rich (1996) obtained an HST/WFPC2 colour magnitude diagram (CMD) reaching about 2 magnitudes below the oldest main sequence turnoff. By analysing the distribution of stars near the base of the red giant branch (RGB), they determined that the

[*] E-mail: marco.gullieuszik@oapd.inaf.it

Table 1. Observing Log

Filt.	N_{ima}	DIT(s)	N_{exp}	N_{jit}	microsteps
J	6	5.0	2	9	2×2
H	6	5.0	2	9	2×2
K_s	10	5.0	2	9	2×2

first generation of stars in Leo II was coeval with the formation of Galactic Globular clusters, and nearly half of the stars formed during a period of star formation lasting about 4 Gyr, with the typical star forming about 9 Gyr ago. They found a negligible rate of star formation in the last ~ 7 Gyr. Subsequent re-analyses of these data confirmed this scenario and found a star formation history (SFH) dominated by old stellar populations with a low star formation rate in the last 8 Gyr (Hernandez et al. 2000; Dolphin 2002; Dolphin et al. 2005). A recent wide-field study has shown a gradient in the HB morphology and the mean age of stellar populations, with a significant population younger than 8 Gyr found only at the centre (Komiyama et al. 2007).

The presence of a small intermediate age population in Leo II is also indicated by a small number of C stars (Aaronson, Hodge, & Olszewski 1983; Aaronson & Mould 1985; Azzopardi, Lequeux & Westerlund 1985). Azzopardi et al. (1985) list six certain C stars and one candidate, while Azzopardi (2000) stated they found two new ones but without providing further details.

As part of an imaging study of Local Group (LG) dwarf galaxies in the near infrared (NIR), we have undertaken a study of the evolved stellar populations in Leo II using wide-area NIR imaging. The main goals are to study the metallicity distribution of red giant stars and to obtain J, H, and K_s magnitudes of asymptotic giant branch (AGB) stars (Gullieuszik et al. 2007a,b). The main advantage of NIR observations for studying AGB stars over the alternative search technique based on intermediate band imaging in the optical (Albert, Demers & Kunkel 2000; Battinelli & Demers 2000; Nowotny et al. 2001), is that the spectral energy distribution of cool AGB stars peaks in the NIR (e.g., Gullieuszik et al. 2007a). Also, bolometric corrections are smaller and more precise in the NIR making comparison with theoretical quantities easier. In addition, the (foreground and internal) extinction is much lower in the NIR than in the optical (Rieke & Lebofsky 1985).

2   OBSERVATIONS AND REDUCTION

Observations of Leo II were carried out in April 19–20, 2005 using the wide-field NIR camera WFCAM at the UKIRT telescope on Mauna Kea, Hawaii. WFCAM uses 4 Rockwell Hawaii-II HgCdTe detectors with a pixel scale of $0''4$ pixel^{-1}. The size of each array is 2048×2048 pixels, corresponding to about $13'6 \times 13'6$, and the 4 arrays are separated by a gap comprising 94% of the detector size. Since the area encompassed by one array is comparable to the galaxy size , we used only one array (No. 3) to observe Leo II. The remaining detectors provide a useful estimate of the foreground/background counts.

Each "observation" (or pointing) consisted of 4 micro-stepped 10 s images (two 5 s coadds) on a 9-points jitter pattern, totalling a 360 s exposure time. In total, 6 observations were obtained in J and H and 10 in the K_s band, yielding a total on-target integration time of 36 min in J and H and 1 h in K_s. The 2×2 "small" microstepping was used to obtain a better spatial sampling. The observing log is given in Table 1.

The raw data were processed using the WFCAM pipeline provided by the VISTA Data Flow System Project, to which the reader is referred for details (Dye et al. 2006). The pipeline combines the micro-stepped images in each band into 4k×4k "Leavstack" oversampled images with a spatial resolution twice that of the original raw images, i.e. $0''2$ pixel^{-1}. The pipeline products are astrometrically calibrated using the ZPN projection (Calabretta & Greisen 2002) and the 2MASS Point Source Catalogue (PSC, Skrutskie et al. 2006) as a reference, with a final systematic accuracy of the order $0''1$. In our analysis, we made use only of the array where Leo II had been centred (No. 3) along with a second array (No. 2) used to estimate the contribution of the foreground Galactic stars and background galaxies.

Point spread function (PSF) photometry was performed on the individual oversampled images (6 in J and H, 10 in K_s) using the ALLSTAR/ALLFRAME (Stetson 1987, 1994). The PSF was generated with a Penny function with quadratic dependence on the position on the frame. The final catalogue includes instrumental PSF magnitudes of objects detected in at least 2 images in 2 bands.

The positions of the sources in the raw photometric catalogue were converted from pixels to the J2000 equatorial system using the astrometric calibration provided by the pipeline and IRAF[1] tasks including support for the ZPN projection.

The final, calibrated NIR photometric catalogue of stars in Leo II is provided in the electronic version of the journal. A few lines are presented in Table 2 to illustrate its content.

Artificial star experiments were also performed to evaluate the photometric errors and completeness of our photometry. We performed 20 test runs adding ~ 2000 stars on a $2k \times 2k$ portion of the frames. The input magnitudes and colours were randomly generated to reproduce the RGB of Leo II. The results of our experiments (completeness factor and internal r.m.s. photometric errors) are shown in Fig. 2. The completeness factor is larger than 50% for magnitudes brighter than $K_s \simeq 20$. Note, however, that most results of this paper are based on photometry of stars brighter than $K_s \simeq 18$, for which we have a completeness factor $\simeq 100\%$ and photometric errors smaller than 0.02 mag.

Possible spatial variations in the completeness factor and photometric errors were investigated by repeating the analysis of artificial star experiments for different regions of our frames, and no significant variation was found. In fact, our scientific photometric catalogue only contains ~ 3200 objects, hence we expect spatially-varying crowding effects

---

[1] The Image Reduction and Analysis Facility (IRAF) software is provided by the National Optical Astronomy Observatories (NOAO), which is operated by the Association of Universities for Research in Astronomy (AURA), Inc., under contract to the National Science Foundation.
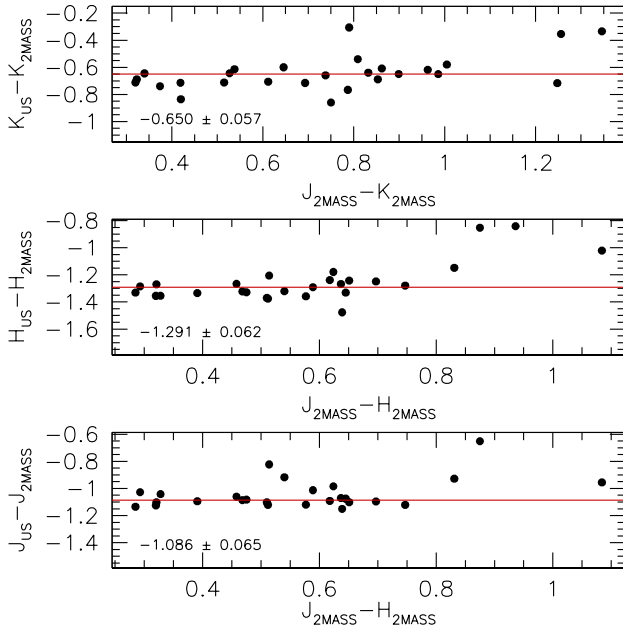
Figure 1. Comparison of Leo II WFCAM instrumental magnitudes corrected using the Dye et al. (2006) colour terms with 2MASS photometry, for stars in common with the 2MASS PSC. No residual colour terms are detectable. In each panel the median difference and the standard deviation of the data are shown.

Table 2. The NIR catalogue of Leo II stars over WFCAM array No. 3. A few lines are shown here for guidance regarding its form and content, while the full catalogue is available from the electronic edition of the journal. .

ID	α (J2000)	δ (J2000)	J	H	K_s
1	11:13:26.53	+22:02:09.7	21.01	19.38	19.41
2	11:13:11.40	+22:02:10.2	19.97	19.13	18.26
3	11:13:11.68	+22:02:12.1	20.00	19.13	18.25
4	11:13:45.11	+22:02:14.3	20.55	19.21	18.45
5	11:13:29.49	+22:02:19.0	20.63	19.81	18.75

to be unimportant. The effect of a photometric bias towards brighter retrieved magnitudes, caused by photometric blends (e.g., Gallart et al. 1996), was also investigated and found negligible (in our experiments the mean difference is always less than 0.01 mag for stars brighter than $K_s \simeq 18$).

3 COLOUR-MAGNITUDE DIAGRAMS

Figure 3 presents our $J-K_s$, K_s colour-magnitude diagram of Leo II, along with optical–NIR CMDs and an optical $B-V$, V CMD. A selection based on the SHARP parameter was applied to remove noise peaks, diffuse objects, and other spurious detections . The optical–NIR CMDs and the optical CMD were obtained by adding data obtained with the EMMI camera at the NTT at ESO/La Silla (Momany et al. 2007, Rizzi et al., in prep.). Since the optical photometry refers to a smaller central area ($9'.1 \times 9'.1$ in V, $6'.2 \times 6'.2$ in B), all diagrams involving optical data refer to a subset of our WFCAM catalogue.
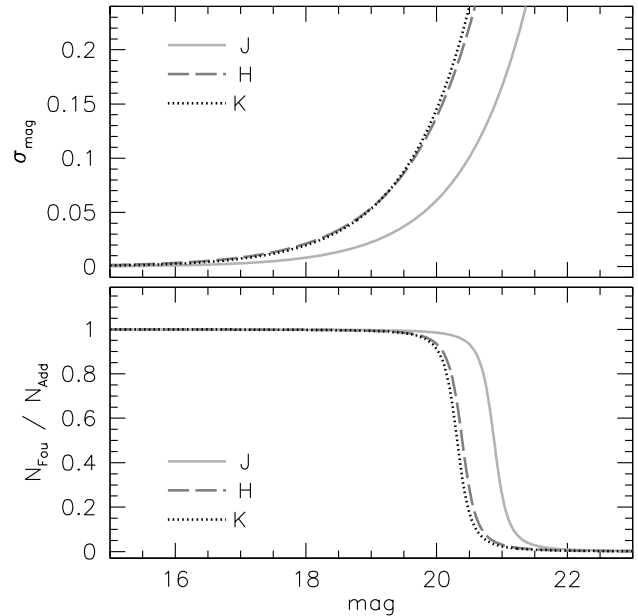

Figure 2. Completeness (*lower panel*) and photometric errors (*upper panel*) in our Leo II images as derived from artificial star experiments, plotted against the input magnitudes of simulated stars.

Our NIR CMD of Leo II shows a well populated RGB, with an TRGB clearly visible at $K_s \sim 16$. Two 10 Gyr old isochrones (Girardi et al. 2002), with metallicity $Z = 0.001$ and $Z = 0.0004$ (corresponding to [Fe/H] ~ -1.3 and [Fe/H] ~ -1.7), are superimposed to the CMD. The CMD almost reaches the level of the HB, identified with the tail of faint stars with colours bluer than the RGB, at a magnitude which is consistent with $V_{HB} = 22.18 \pm 0.18$ measured by Mighell & Rich (1996). However, these stars will not be further analysed since they fall close to the detection limit in the CMD.

The sequence of stars brighter than the TRGB ($K_s \sim 15$) is identified with upper-AGB stars belonging to an intermediate-age stellar component. These stars appear to coincide with the sample of C stars identified by Azzopardi et al. (1985). Note that they are more luminous than the TRGB only in the $J-K_s$, K_s diagram, while they appear progressively fainter in bluer photometric bands. This C star population is quite small, in agreement with the low star formation rate of Leo II at intermediate ages. The AGB population will be further discussed in Sects. 6 and 7. The candidate C star with uncertain classification in Azzopardi et al. (1985) does not share the spectral energy distribution of the C stars in the different CMDs. Visual inspection of our images confirms that it as a background galaxy.

Note that both the prominent RGB sequence and the AGB component are absent in the CMD of an outer field of Leo II, obtained from the detector No. 2 of WFCAM (Fig. 4). This field is located at about $26'$ from the centre of Leo II, corresponding to about 3 tidal radii. A comparison with a simulation of the Galactic foreground, obtained for the same field-of-view using the TRILEGAL code (Girardi et al. 2005), is shown in the right panel of Fig. 4. The comparison in-
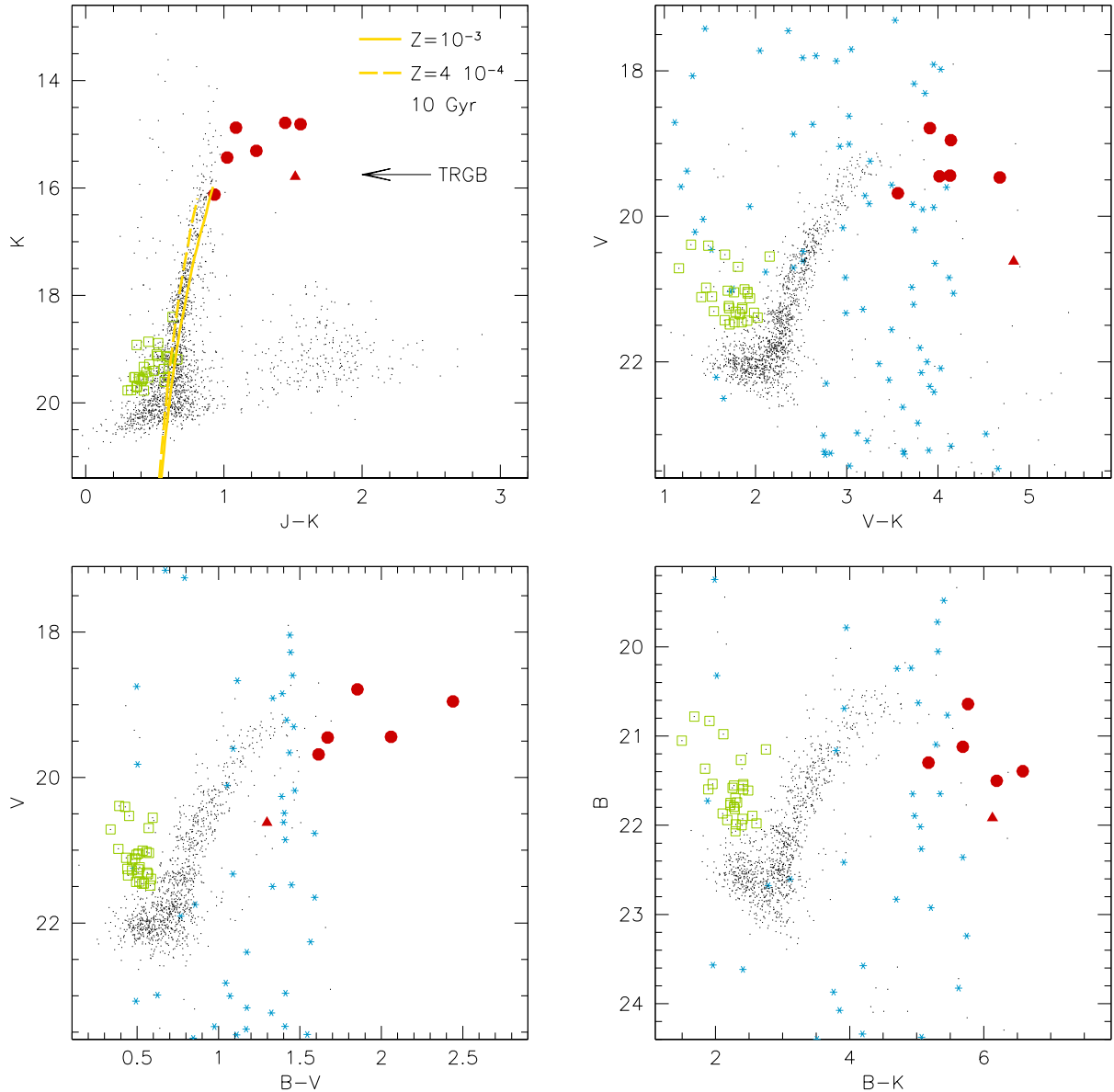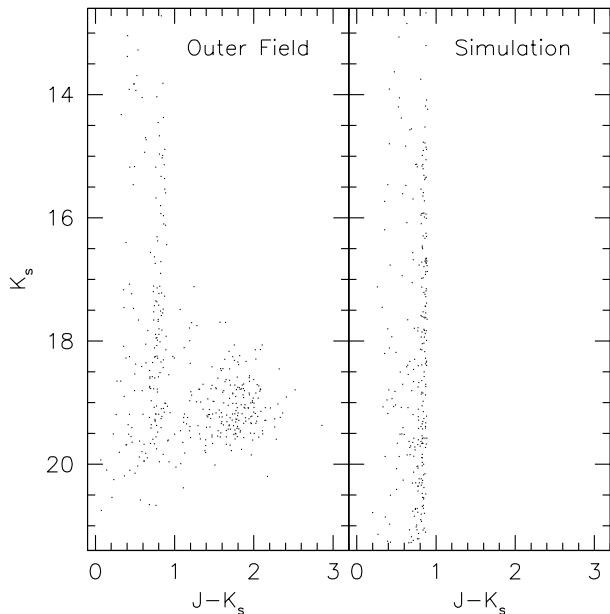
Figure 3. Colour-magnitude diagrams of Leo II from NIR and combined optical-NIR photometry. In all diagrams, C stars spectroscopically identified by Azzopardi et al. (1985) are shown as *filled circles*, while their C star uncertain candidate is marked by a *triangle*. Superimposed on the $J-K_s$, K_s CMD are theoretical isochrones from Girardi et al. (2002), for an age 10 Gyr and two metallicities close to the metallicity of Leo II, $Z = 0.001$ and $Z = 0.0004$. In all except the $J-K_s$, K_s CMD, we also show as *asterisks* the predicted Galactic foreground stars towards Leo II from a TRILEGAL simulation (Girardi et al. 2005). The He-burning stars on the "yellow plume", selected from the optical $B-V$, V diagram, are shown as *open squares*. They are best seen in the $B-K_s$, B diagram, whereas the same stars are confused with the RGB in the $J-K_s$, K_s CMD.

dicates that the CMD of the outer region mostly contains Milky Way stars (the vertical sequence with $J-K_s \sim 0.8$ and bluer objects) and background galaxies (concentrated at $J-K_s > 1$, $K_s > 18$).

The wide baseline of optical–NIR diagrams provides the best separation of some CMD features. In Fig. 3, we plot as open squares the stars on the "yellow plume" or "vertical clump" (VC), just above the red clump, according to a magnitude and colour selection from the optical $B-V$, V diagram. These stars are best seen in the $B-K_s$, B diagram as a vertical sequence originating from $B-K_s \sim 2.5$, $B \sim 22.5$

and extending up to $B \sim 21$; while they are hardly detected in the $J-K_s$, K_s NIR diagram, an ambiguity that is explained by a combination of increasing photometric errors at faint magnitudes and an intrinsically narrow baseline.

The distribution of these "vertical clump" stars can be compared in Fig. 3 with the distribution of Milky Way foreground stars in the direction of Leo II, obtained from the TRILEGAL code (Girardi et al. 2005). The projected Galactic contamination (plotted as starred symbols) is insignificant in the yellow plume region of the $B-K_s$, B diagram, indi-

Figure 4. *Left:* colour-magnitude diagram of an outer field of Leo II, obtained from the detector No. 2 of WFCAM, pointing at about $26'$ from the centre of Leo II. The vertical sequence having $J-K_s \lesssim 0.8$ is consistent with the expected Galactic foreground, while the group of objects redder than $J-K_s = 1$ and fainter than $K_s = 18$ are unresolved background galaxies. *Right panel:* Milky Way stars in the Leo II line of sight as derived from a TRILEGAL simulation (Girardi et al. 2005), for the observed field-of-view, without photometric errors.

Table 3. Observed magnitude of the TRGB and distance moduli derived for Leo II from JHK_s photometry.

band	m^{TRGB}	$(m-M)_0$	$err_{(m-M)_0}$
J	16.67	21.73	0.17
H	15.90	21.69	0.19
K_s	15.75	21.58	0.21

cating that the vertical sequence is certainly a Leo II stellar population.

In dwarf galaxies, this feature is usually attributed to a population of core He burning stars a few hundred Myr to ~ 1 Gyr old, which are the descendants of stars located above the old main-sequence turnoff, the so-called blue plume. Thus, the detection of VC stars is generally interpreted as evidence of recent star formation in these galaxies (e.g., in Draco: Aparicio, Carrera & Martínez-Delgado 2001). This is probably the case for Leo II, where there is evidence for an increasing number of young stars toward the centre (Komiyama et al. 2007). However, there is some evidence that the detection of a VC sequence in dwarf spheroidal galaxies may not be sufficient to establish the presence of recent star formation (Momany et al. 2007; Mapelli et al. 2007), since stars brighter than the HB have been detected in globular clusters (see the case of M80 in Ferraro et al. 1999). The agreement of the "blue plume" frequency in 7 dwarf spheroidal galaxies (including Leo II) might be a hint that this population is partly comprised of "blue stragglers", of which the VC population may represent the evolved counterparts.

4 DISTANCE FROM THE RGB TIP

The luminosity of the TRGB in the I band (where the dependence on the age and chemical composition of the stellar population is at a minimum) has long been used as a valuable standard candle (Da Costa & Armandroff 1990;

Lee et al. 1993). In the NIR, the TRGB luminosity depends on age and metallicity in a more complex way. For instance, the K_s-band magnitude of intermediate-age stars at the TRGB is fainter than that of old stars; while the TRGB K_s luminosity rises with increasing metallicity (e.g., Salaris & Girardi 2005). For a population that becomes more metal-rich with time as a result of galaxy chemical evolution, the two effects can partly balance. In Gullieuszik et al. (2007a) we showed that, if the galaxy's SFH can be (even roughly) estimated, quite accurate distance determinations can be obtained from the TRGB at NIR wavelengths.

The method is applied here to measure the distance to Leo II independently of optical measurements. This will also be a useful test of the reliability of distance estimates in the NIR domain, which is important for next-generation instruments operating mainly at NIR wavelengths (e.g., JWST, adaptive optics at Extremely Large Telescopes).

We estimated the magnitude of the TRGB of Leo II by fitting its K_s-band luminosity function to a step function convolved with a Gaussian kernel representative of the photometric errors. This method, extensively applied by our group (e.g., Momany et al. 2002), was found to give consistent results within 1σ with the Maximum Likelihood Algorithm of Makarov et al. (2006) (see Rizzi et al. 2007). The resulting J, H, and K_s magnitudes of the TRGB are given in Table 3. The errors associated to these magnitudes are dominated by the uncertainty on the absolute photometric calibration, because the error resulting from the TRGB fitting algorithm is less than 0.01 mag, and the internal photometric errors at the level of the TRGB are negligible (see Sect. 2). The observed magnitude were corrected for extinction using a reddening $E_{B-V} = 0.03$ and the Rieke & Lebofsky (1985) reddening law.

To derive the distance to Leo II, the JHK_s TRGB magnitudes were compared with the empirical calibrations of $M_\lambda^{\mathrm{TRGB}}$ as a function of [M/H] based on Galactic globular clusters (Valenti et al. 2004b), whose intrinsic systematic error is $\sigma = 0.16$ mag. The adopted mean metallicity was [M/H] $= -1.73$, in agreement with Koch et al. (2007) spectroscopy. Given the relatively old age distribution of Leo II, we found the population corrections (calculated as in Gullieuszik et al. 2007a) to the TRGB magnitude to be negligible.

The distances derived from the J, H, and K_s bands are also given in Table 3. The weighted mean is $(m-M)_0 = 21.68 \pm 0.11$, and intermediate between the "short" distance $(m-M)_0 = 21.55$ obtained by Mighell & Rich (1996) from the V magnitude of the HB and the "long" distance $(m-M)_0 = 21.84 \pm 0.13$ derived by Bellazzini et al. (2005) from the I magnitude of the TRGB. Therefore, our determi-
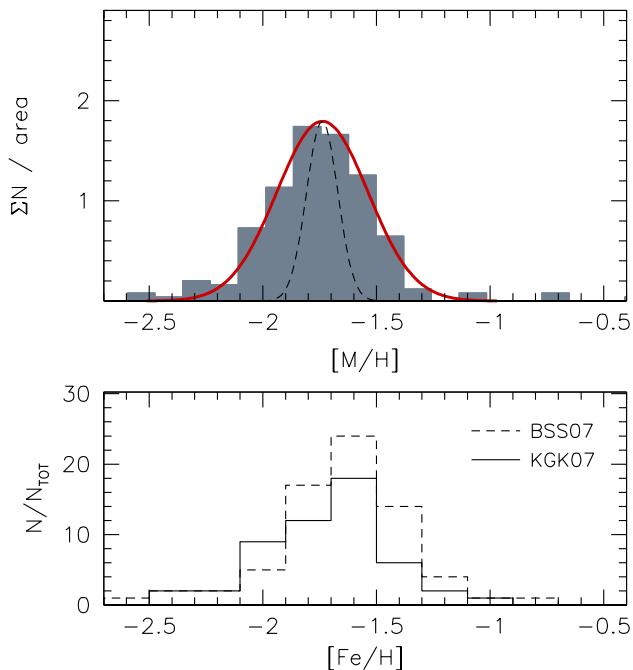
Figure 5. *Upper panel:* the photometric Metallicity Distribution Function of RGB stars in Leo II, constructed using global metallicities [M/H] derived from $(V - K_s)$ colours. The *solid line* is a Gaussian fit to the data, with mean [M/H] $= -1.74$ and $\sigma_{[M/H]} = 0.20$ dex. The measurement scatter is represented by a Gaussian with $\sigma_{instr} = 0.06$ dex (*dashed curve*). *Lower panel:* the spectroscopically derived MDFs of Koch et al. (2007) (*solid line*) and Bosler et al. (2007) (*dashed histogram*), both on the Carretta & Gratton (1997) scale.

nation based on NIR magnitudes of the TRGB appears to be consistent, within the errors, with the optical estimates. The techniques explored in this paper will be useful to measure the distance of stellar systems for which photometry of resolved stars will become available only in the NIR.

5   METALLICITY

5.1   Metallicity distribution of RGB stars

Given the uncertainties on the metallicity of Leo II and the importance of the metallicity distribution function (MDF) of RGB stars as a constraint on models of chemical evolution of dwarf galaxies, we used all the information from optical–NIR colours to investigate the metallicities of stars in Leo II. This parameter is the most appropriate to estimate the metallicities of dwarf spheroidal galaxies (having $[\alpha/Fe]$ ratios close to solar) by comparison with the photometric properties of Milky Way globular clusters, which generally show an overabundance of α-elements relative to iron that is a function of the cluster metallicity (see Geisler et al. 2007, and refs. therein).

The photometric MDF obtained for red giant stars in Leo II down to 2 mag below the TRGB, is shown in Fig. 5 (upper panel). The distribution is well described by a Gaussian function centred at [M/H] $= -1.74$ and with a measured dispersion of 0.20 dex. The internal error in the same mag-

nitude range was evaluated by applying the same method to a synthetic CMD simulating a thin RGB, taking into account the results of artificial star experiments. The recovered metallicities have a Gaussian distribution with a dispersion 0.06 mag, assumed to be representative of the internal error of our metallicity measurements. By quadratically subtracting this internal error from the measured width of the MDF, we obtain a corrected dispersion 0.19 dex for the photometric MDF of Leo II.

Our photometric MDF shown in Fig. 5 is representative of the *true* MDF only for stars as old as the Galactic GCs (~ 12.5 Gyr). However, a typical Leo II star is 9 Gyr old (e.g. Mighell & Rich 1996), hence slightly bluer than globular cluster stars of the same metallicity. Therefore, as in Gullieuszik et al. (2007a), we used theoretical isochrones to construct contours of constant $V - K_s$ colours of RGB stars, as a function of both stellar age and metallicity, and correct the measured metallicity for the age effect. This is done by estimating the metallicity of a 9 Gyr old star having the same colour as a 12.5 Gyr star with [M/H] $= -1.74$, i.e. the mean of the MDF. This differential approach overcomes any possible problems with the absolute calibration of the isochrone colours. With this assumption, the age correction results to be $\Delta[M/H] = 0.10$, which is very small and comparable with the absolute uncertainty of our method. Our major simplification is that *all* stars have the same age, but it is adequate to calculate the *mean* metallicity of Leo II stars. By applying this correction, the mean metallicity of Leo II turns out to be [M/H] $= -1.64 \pm 0.06$ (random) ± 0.17 (systematic).

5.2   Comparison with spectroscopy

The derived metallicity is in excellent agreement with the two recent spectroscopic results [Fe/H] $= -1.73$ and $= -1.59$ by Koch et al. (2007) and Bosler et al. (2007), respectively. Our metallicity distribution of Leo II RGB stars, as inferred from $V - K_s$ colours, is compared with the spectroscopic metallicity distributions from Bosler et al. (2007) and Koch et al. (2007) in Fig. 5 (lower panel). The distributions are basically consistent, except for a slightly lower mean metal abundance from photometry. In particular, the range in metallicity (FWHM of the distributions) is comparable.

The significant overlap between our sample of RGB stars and the catalogues of Bosler et al. (2007) and Koch et al. (2007) allows us a direct comparison of photometric and spectroscopic metallicity estimates on a star-by-star basis.

Figure 6 shows a comparison with the results of Bosler et al. (2007), for 71 stars in common with our sample. In the metallicity range typical of Leo II stars, the two calibrations adopted by those authors (as a function of [Fe/H] and [Ca/H]) yield [Fe/H] $\simeq$ [Ca/H]. Indeed, the relations presented in Fig. 6 for the two scales are quite similar. For both scales, the overall agreement between spectroscopic and photometric metallicities appears to be good. The most noteworthy difference is for the bluest stars, whose spread is higher and spectroscopic metallicities are systematically higher. A possible explanation is that the photometric metallicities are underestimated because some stars are actually younger (hence bluer) than old RGB stars. One alternative possibility is that calibration uncertainties and
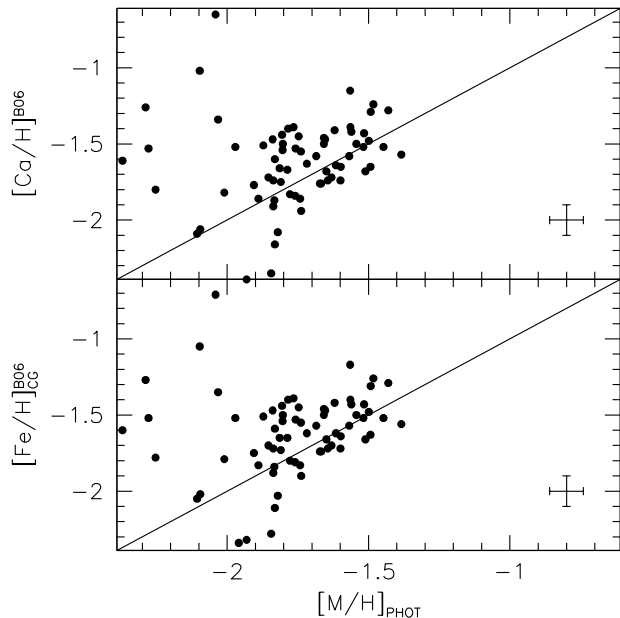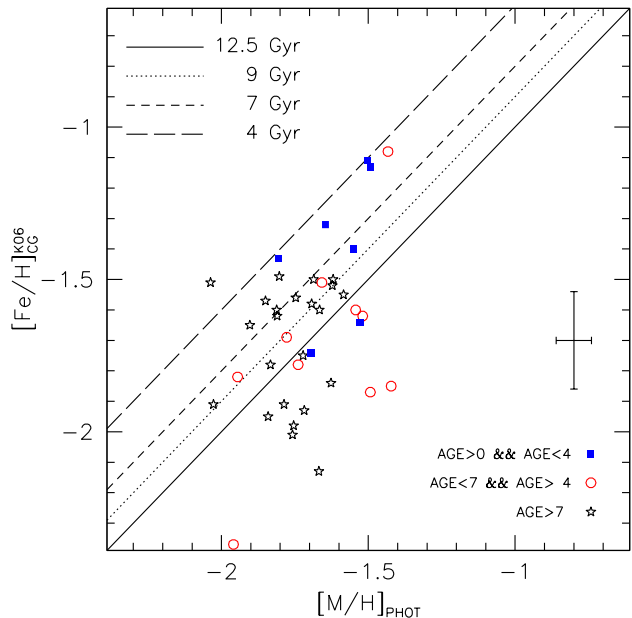
Figure 6. Comparison of our measured photometric metallicities with the spectroscopic results of Bosler et al. (2007). In the *upper panel* we plot the spectroscopic data on the [Ca/H] scale of the authors, while the calibration based on [Fe/H] is shown in the *lower panel*. The error crosses represent the mean uncertainties of spectroscopic metallicities, and the 1σ internal errors of our photometric determinations (not including age effects and systematic uncertainties).

Figure 7. Comparison of individual stellar metallicities with those derived by Koch et al. (2007), using different symbols for stars in different age intervals, as estimated by Koch and coll. The lines represent the expected relations when the effects of age on $V-K_s$ colours are taken into account. For example, 4 Gyr old stars are expected to follow the long-dashed line. Error bars as in Fig. 6.

internal errors affect in some way the spectroscopic measurements at low metallicity.

A comparison of our photometric metallicities (with no age correction applied) with the spectroscopic results of Koch et al. (2007) is presented in Fig. 7. The 41 stars in common with our sample are divided in 3 age intervals, using the age estimates published by Koch et al. (2007). The stars with ages (as derived by Koch et al. 2007) greater than 7 Gyr, and most of the stars with ages in the range 4 to 7 Gyr, are broadly consistent, with a large scatter, with the bisector in Fig. 7, i.e. compatible with the age of Galactic globular clusters.

We have also plotted the age-corrected relations (represented by different lines in Fig. 7), by calculating the metallicity shifts to be applied to our photometric measures for young stellar populations. Assuming an age of 9, 7, and 4 Gyr, the corrections are $\Delta[\mathrm{M/H}] = 0.10$, 0.20, and 0.41, respectively. Indeed, the location of stars younger than 4 Gyr seems consistent with the expected relation for 4 Gyr old stars. In general, however, we note a sizeable scatter, even considering stars within each age bin, and the ages estimated by Koch et al. (2007) do not appear to be closely correlated with the age-corrected relations in Fig. 7. Overall, the number of young stars in Leo II derived by Koch et al. (2007) appears to be larger than suggested by SFH reconstructions based on HST photometry (Hernandez et al. 2000; Dolphin 2002, Rizzi et al., in prep.), and the mean age of RGB stars is younger. We note that our age corrections, based on the larger baseline of $V-K_s$ colours, may give more precise age ranking than the $g-i$ colour used by Koch et al. (2007).

A direct comparison of spectroscopic metallicities, which would be interesting to assess the accuracy of spectroscopic metallicities, is not possible due to the absence of overlap between the samples of Koch et al. (2007) and Bosler et al. (2007).

6 TWO-COLOUR DIAGRAMS: SELECTION OF AGB STARS

In this section we present the two-colours diagram, which is used to select AGB stars in Leo II. This diagram is a powerful tool to separate the foreground Milky Way stellar population, and allows a separation of carbon and oxygen-rich stars (Aaronson & Mould 1985; Bessell & Brett 1988).

Figure 8 shows the NIR two-colour diagrams of Leo II and the external field. We selected only stars brighter than the TRGB ($K_s = 15.75$) to exclude RGB stars. Stars are located in well defined sequences, within the regions outlined in Fig. 8. All stars located in regions 2 and 3 are found along the dwarf stars locus defined by Bessell & Brett (1988). The number of stars in each region are also given in Fig. 8 for the field centred on Leo II and the external field. The number of stars in regions 2 and 3 are the same, within statistical fluctuations, in the two fields. We can therefore conclude that *all* stars in regions 2 and 3 are Milky Way dwarfs. On the other hand, stars in region 1 and 4 are found only in the field centred on Leo II, and we can conclude that they are all Leo II members. Being brighter than the TRGB, they can only be AGB stars. For stellar populations younger than those present in Leo II, core He-burning red supergiants should be also considered.
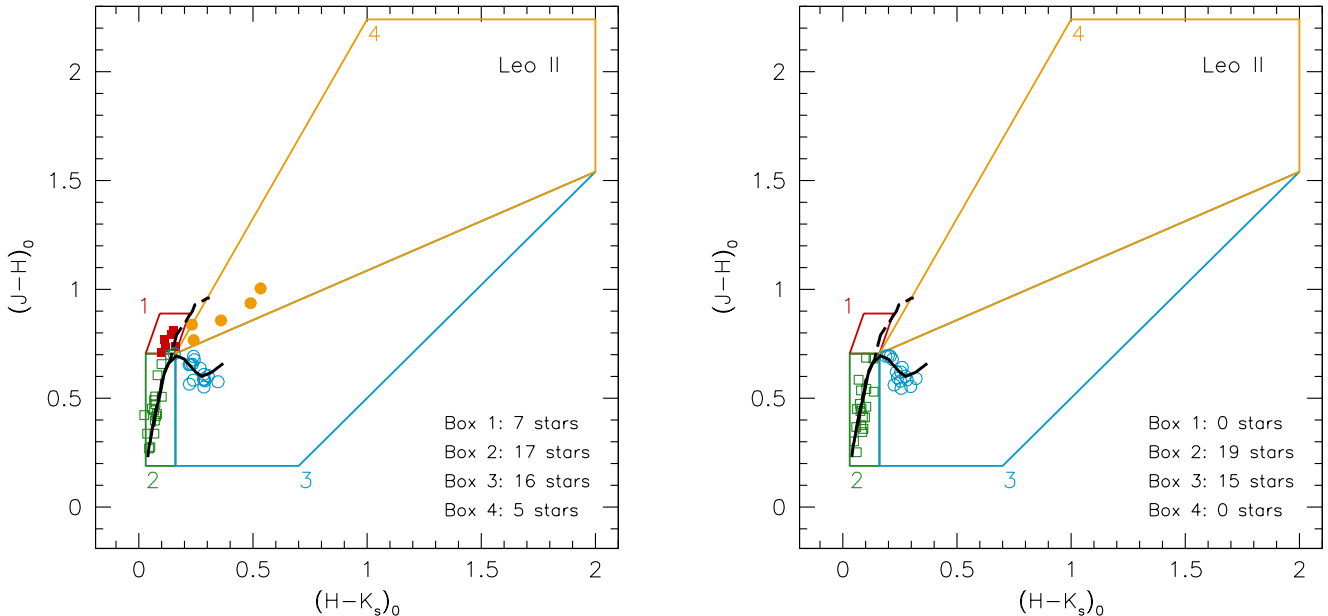
Figure 8. *Left Panel:* the two-colour diagram of Leo II stars brighter than the TRGB ($K_s = 15.75$), with superimposed the regions we have used to discriminate stars in Leo II from those in the Milky Way: region (1) are probable Leo II O-rich AGB stars, regions (2) and (3) are dwarf Galactic stars, region (4) is populated by C stars in Leo II. Different symbols indicate stars in different regions. The loci of giant stars and main-sequence dwarf stars (from Bessell & Brett 1988) are shown as a *dashed* and *solid line*, respectively. *Right Panel:* the same, for the outer field. Note the absence of stars belonging to Leo II.

All of the five stars in region 4 were identified as C stars by Azzopardi et al. (1985). One more C star in their catalogue (ALW5) is slightly fainter than the TRGB (see Fig. 3) and hence is not marked in Fig. 8. If plotted, it would fall in region 3.

Figure 9 shows the location in the CMD of the stars classified using the NIR two-colour diagram. Stars in the regions 1 and 4 are consistent with the expected loci of M and C stars respectively, as judged from the location of AGB stars with spectroscopic classification in the CMD of Fornax dSph (see Gullieuszik et al. 2007a, and ref.s therein). The C star population, in particular, agrees well with the mean colour-magnitude relation for C stars in LG dwarf galaxies derived by Totten et al. (2000), scaled to the distance of Leo II discussed in Sect. 4. NIR photometry of all C stars classified by Azzopardi et al. (1985) and probable O-rich AGB stars selected by us in region 1, is given in Table 4.

In the following, we consider all the C stars identified by Azzopardi et al. (1985), including star ALW5, which is fainter than the TRGB and was therefore not included in Fig. 8. The objects ALW2, misidentified by Azzopardi et al. (1985) as a C star, is not included in our analysis. All the remaining stars by Azzopardi et al. (1985) are compatible with our C star selection and our observations cover all Leo II, nearly out to the tidal radius. We therefore conclude that the complete population of Leo II C stars in the central $13'.6 \times 13'.6$ area covered by our observations, is formed by 6 objects (excluding ALW2). We finally note that Azzopardi (2000) stated they found 2 new ones but without providing further details. In our selection we have no indications for the presence of other objects in addition to the 7 discussed

here. Finally we consider as O-rich AGB stars the 7 stars found in region 1 in Fig. 8.

7   COMPARISON WITH THEORETICAL MODELS

A distinctive feature of present observations is that they sample quite completely the optically-visible AGB population of Leo II in the surveyed area. The only AGB stars expected not to be present in our data are those so strongly absorbed by circumstellar dust to become invisible even in the NIR.

Such complete catalogues of AGB stars in nearby galaxies are rare. The best such data are no doubt those for the LMC and SMC, fully sampled in the $IJHK_s$ bands of DENIS and 2MASS (see Cioni et al. 1999; Nikolaev & Weinberg 2000) and now being sampled in the mid-IR (e.g Blum et al. 2006; Bolatto et al. 2007). Compared to these galaxies, Leo II is more metal-poor (Sect. 5), and presents a much simpler history of star formation, concentrated at old ages. These particularities provide us with a unique opportunity to test present-day AGB models in the interval of low masses and low metallicities.

7.1   Simulating the photometry

Having this goal in mind, we will try to fit the Leo II observed AGB population with the recent set of thermally pulsing AGB (TP-AGB) evolutionary tracks from Marigo & Girardi (2007). Added to the Girardi et al. (2000) tracks for the pre-TP-AGB evolution, they are converted to stellar isochrones as described in
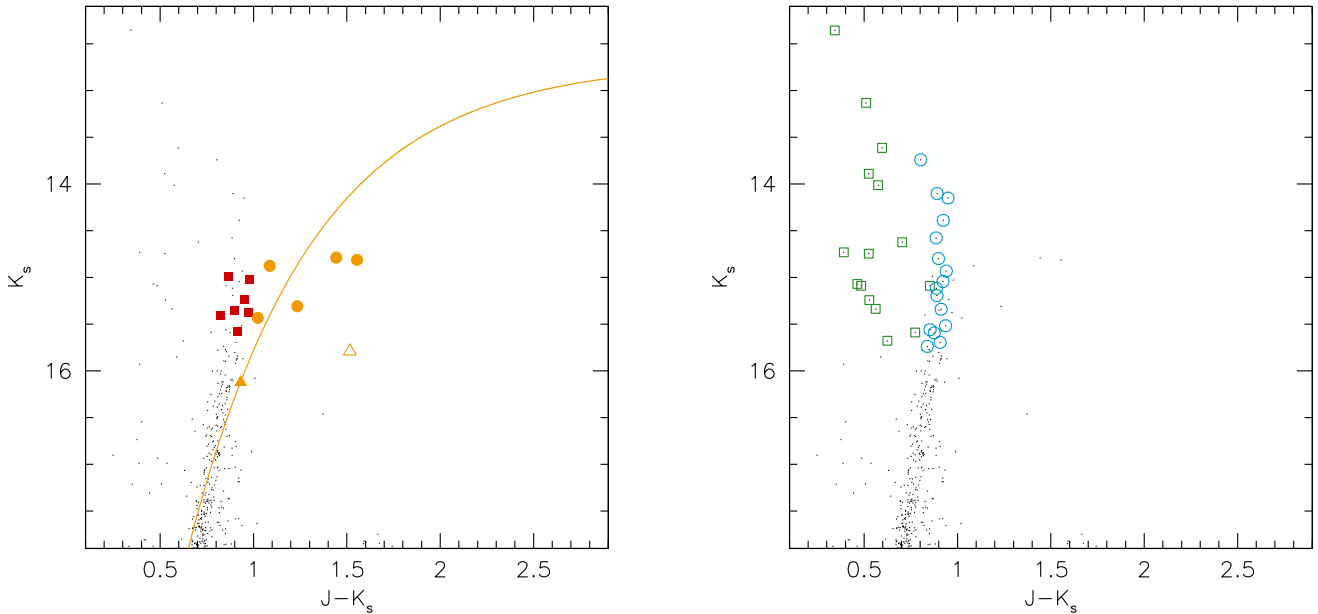
Figure 9. The position of Leo II and foreground stars in the CMD according to the classification shown in Fig. 8 for stars brighter than the TRGB. *Left:* stars in the regions 1 (*squares*) and 4 (*filled circles*). The *open triangle* represents ALW2, a misidentified background galaxy, while the *filled triangle* is a C star found just below the TRGB (ALW5, Azzopardi et al. 1985). The *solid curve* is the mean colour-magnitude relation for C star in Local Group dwarf galaxies (Totten et al. 2000), scaled to the distance of Leo II. *Right panel:* the same, for probable Milky Way stars in the regions 2 (*open squares*) and 3 (*open circles*) of the two-colour diagram.

Table 4. NIR photometry of Leo II AGB stars. The identifiers are those in our photometric catalogue. For the C stars, the names in Azzopardi et al. (1985) are also given.

ID	α (J2000)	δ (J2000)	J	H	K_s	type	note
1661	11:13:12.82	+22:11:14.1	16.231	15.284	14.788	C	ALW1
1671	11:13:20.64	+22:11:16.3	16.366	15.351	14.812	C	ALW3
659	11:13:23.48	+22:07:58.4	16.542	15.674	15.308	C	ALW4
828	11:13:23.97	+22:08:29.3	17.054	16.365	16.122	C	ALW5
1089	11:13:29.39	+22:09:14.2	15.963	15.114	14.876	C	ALW6
1032	11:13:31.78	+22:09:06.1	16.456	15.679	15.433	C	ALW7
781	11:13:20.83	+22:08:22.9	16.005	15.184	15.027	O	
1215	11:13:35.81	+22:09:35.1	16.252	15.471	15.351	O	
1509	11:13:29.24	+22:10:32.9	16.346	15.531	15.375	O	
1597	11:13:23.16	+22:10:56.0	16.487	15.740	15.574	O	
1873	11:13:53.43	+22:12:43.5	16.229	15.510	15.404	O	
1877	11:13:52.77	+22:12:45.4	15.855	15.113	14.989	O	
1904	11:13:29.17	+22:13:02.7	16.189	15.387	15.236	O	

Marigo et al. (2008) and fed to the TRILEGAL population synthesis code for simulating the photometry of resolved stellar populations (Girardi et al. 2005, http://trilegal.kuleuven.be/). Since the details of the TP-AGB implementation in TRILEGAL are provided in separate papers (e.g. Girardi & Marigo 2007, and work in preparation), suffice here to recall the basic aspects of the model simulations:

• The Milky Way foreground is simulated as in Girardi et al. (2005), including the main disk and halo components and for the same area of our observations.

• The Leo II galaxy is set at a distance of 205 Kpc (this paper). Reddening is ignored since it is negligible.

• We fix the size of the simulations by reproducing the star counts in the upper 2 magnitudes of the RGB – for which our observations are quite complete – together with the relative star formation rate (SFR).

• The relative SFR of Leo II is taken from two different sources, as depicted in the upper panel of Fig. 10: Dolphin et al. (2005) and Rizzi et al. (in prep.). In both cases the SFR is derived from the inversion of a deep CMD from HST. Although the error bars in these SFR determinations are quite significant, these SFRs show that the bulk of star formation in Leo II was confined to ages larger than

2 Gyr, and concentrated at > 4 Gyr. More details are given later.

• The metallicity is taken from the photometric determination of Sect. 5, i.e. we use a Gaussian distribution of mean [M/H]$= -1.64$ and dispersion 0.2 dex. This metallicity distribution is assumed to be the same for all ages, which is likely a good approximation since the age–metallicity relation derived by Koch et al. (2007, their figure 11) is essentially flat for ages above 5 Gyr.

• Each simulated star is converted in the 2MASS system using an updated version of the Bonatto, Bica & Girardi (2004) transformations. In particular, the transformations for carbon stars are now derived from Loidl et al. (2001) spectra. In addition, using Groenewegen (2006) tables we correct the photometry for the effect of circumstellar dust in mass-losing AGB stars. The 60% Silicate + 40% AlOx and 85% AMC + 15% SiC dust mixtures are assumed for O-rich and C-rich stars, respectively.

• For TP-AGB stars, the pulse cycle luminosity and T_{eff} variations are also simulated; long period variability is not. For the high-amplitude Miras, variability may provide an additional scatter of about 1 mag (see, e.g., Cioni et al. 2003) in the K band. Our simulations however predict that most of the AGB stars are first overtone pulsators, which have much smaller amplitudes.

• Photometric errors and completeness are simulated using the relations derived in Fig. 2.

• To reduce the statistic fluctuations in the numbers of predicted stars, each simulation is run at least 50 times with different random seeds. When we refer to the "expected numbers" of each kind of star, we are actually referring to the mean values and standard deviations obtained from these many runs.

Our simulations also take into account the error bars in Dolphin et al. (2005) and Rizzi et al. (in prep.) determinations of the SFH. These error bars reflect both the intrinsic errors in the method of SFR-recovery, and the small number statistics of the original HST data from which the SFR is derived. For each age interval, we use a random SFR value drawn from a normal distribution centred at the mean SFR and with the appropriate value of σ. Since for some age bins the 1σ error bars are comparable to the mean SFR, the negative values of SFR obtained at the youngest age bins are set to zero. This produces a distribution of SFR values that is non-symmetrical around the mean values, especially at the youngest age bins.

One of such simulations is shown in Fig. 11, which resembles very much Fig. 3. First, a key to understand the simulations is given by the Marigo et al. (2008) isochrones for a few selected ages. They show the location of the TP-AGB phase at quiescent phases of H-shell burning, where these stars spend about 70 % of their life. The remaining ~ 30 % is spent at phases of lower luminosity (and higher T_{eff}) after the occurrence of He-shell pulses. The result is that the TP-AGB stars in the simulation are typically found above the TRGB, in the same region defined by the isochrones, but a tail of such objects (both C- and O-rich) extends down to almost 2 mag below it. Moreover, a significant fraction of the O-rich giants found above the TRGB are not genuine TP-AGB stars, but either early-AGB stars or (more rarely,
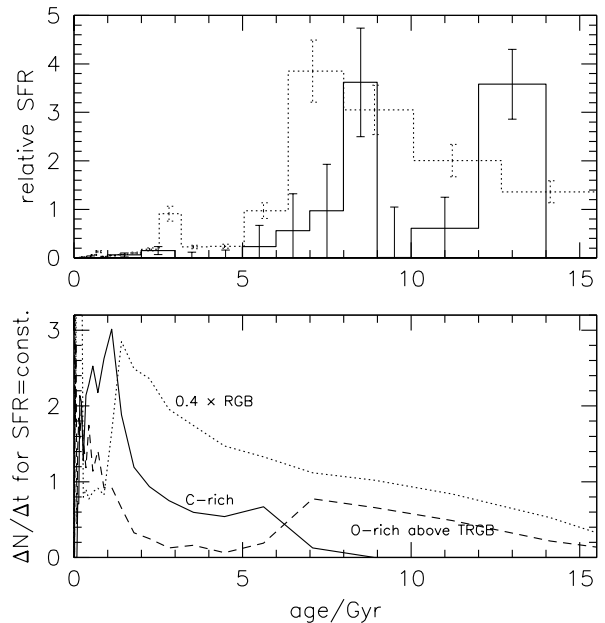
Figure 10. *Top panel:* The star-formation histories used in this work: Dolphin et al. (2005, *dotted line)* and Rizzi et al. (in prep.) (*solid line*) as a function of age. *Bottom panel:* The production (number of stars per time interval) of different types of stars in our models as a function of age, for a galaxy model forming stars at a constant rate (in mass per unit time) from 0 to 15 Gyr, at a constant $Z = 0.0004$ metallicity. The stellar kinds plotted are RGB stars within 2 mag of the TRGB (multiplied by 0.4; *dotted line*), and both O-rich giant stars above the TRGB (*dashed line*) and C-rich giants (*solid line*).

in the case of Leo II) core He burning stars belonging to the youngest populations.

Comparing the simulated data points with the observed ones of Fig. 3, one notices that the main stellar features are accounted for by the model. The simulations do not contain the objects observed at the bottom right part of the diagram ($K_s > 18$, $J-K_s > 1.2$), which likely correspond to background galaxies (e.g. Nikolaev & Weinberg 2000). Simulated carbon stars are on average bluer than the observed ones, although a few very red dust-enshrouded objects are present in our simulations. There are also minor offsets in colours of O-rich stars, that cannot be appreciated in Fig. 11 because they are of the order of 0.05 mag. It is interesting to note that 3 out of the 5 stars expected to be C-rich, are located along the O-rich sequence, i.e., not exhibiting redder $J-K_s$ colours than those of the O-rich stars with the same luminosity. This prediction is consistent with the observed colour-magnitude diagram presented in Fig. 3 (top-left panel), where 3 C-rich objects are just seen to lie on the O-rich giant branch. On the theoretical ground this feature is explained considering that at low metallicity the cooling effect on the stellar atmosphere due to the carbon-enhanced molecular opacity becomes less efficient, as illustrated by Marigo & Girardi (2007, their figure 7).
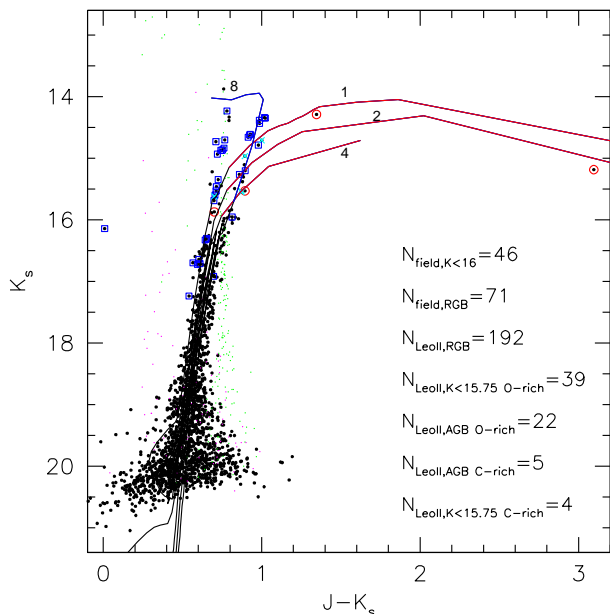
Figure 11. An example of simulated CMDs for Leo II, using the Dolphin et al. (2005) SFH. In the electronic version of this paper, different colours mark different kinds of stars, namely: Milky Way disk (green crosses) and halo (magenta dots), Leo II pre-TP-AGB stars (dark dots), Leo II early-AGB stars above the TRGB magnitude (cyan crosses), and Leo II TP-AGB stars both O-rich (blue squares) and C-rich (red circles). We also plot the Marigo et al. (2008) isochrones for $Z = 0.0004$ and ages of 1, 2, 4, and 8 Gyr, shifted by the Leo II distance modulus. Dark lines mark phases previous to the TP-AGB, blue lines the O-rich TP-AGB, and red lines the C-rich one. The TP-AGB lines correspond to quiescent phases of evolution.

7.2 Comparing foreground and RGB counts

We find that the expected number of foreground stars in our $0.052 \ \mathrm{deg}^2$ area, limited to the $13 < K_s < 16$ magnitude interval, is 38.6 ± 6.8; this is well compatible (within 1σ) with the 44 objects observed in regions 2 and 3 of Fig. 8 at $K_s < 16$. This agreement is just expected, since one of the deep fields used to calibrate TRILEGAL – namely the CDFS (Groenewegen et al. 2002) – is located at the same galactic longitude and at a similar latitude from the Galactic Plane (i.e. $\ell = 220°0$, $b = -53°9$) as Leo II[2]. Therefore, we would expect that the typical errors in the predicted number counts at the position of Leo II ($\ell = 220°2$, $b = +67°2$) are similar to those of the CDFS, i.e. of just ~ 10 % down to $K_s \sim 18$ (see Fig. 6 in Girardi et al. 2005).

As the simulations predict the correct number of foreground stars at $13 < K_s < 16$, they can also be used to infer the field contamination of other CMD regions. We find that a total of 62.0 ± 7.2 foreground stars are expected to contaminate the uppermost 2 mag of the RGB. The total observed number is 254. Therefore, Leo II genuine RGB stars are expected to be about 192 and outnumber the foreground contaminants in the upper part of the RGB by a factor of about 4. If we assume the possible errors in the number of

---

[2] Note that number counts in NIR bands are very much symmetrical with respect to the Galactic Plane, at least for $|b| \gtrsim 20$ deg.

---

simulated foreground stars to be of the order of 20 percent, they will have just modest consequences (errors of the order of 8 %) in determining the total Leo II mass to be simulated.

7.3 Comparing AGB counts

We proceed with Leo II simulations with a total mass scaled such as that 192 ± 14 RGB stars are produced in the upper 2 magnitudes of the RGB. The results concerning the AGB are as follows.

For the Rizzi et al. (in prep.) SFR, we expect to find 43.9 ± 6.6 O-rich giants above the TRGB (with 29.4 ± 5.5 being genuine TP-AGB stars). The C-rich AGB stars are 4.4 ± 2.4 (with 3.4 ± 2.2 above the TP-AGB). In comparison, the Leo II data presents 7 and 6 of such stars, respectively. There is a clear excess of O-rich giants in the simulations, by a factor of about 6, which is extremely unlikely to be due to statistical fluctuations. For the C stars, instead, getting 6 stars out of an expected number of 4.4 is well inside the 67 % confidence level (CL) of a Poisson distribution.

Using the Dolphin et al. (2005) SFH, 42.0 ± 5.5 O-rich giants are predicted above the TRGB (26.4 ± 4.7 genuine O-rich TP-AGB ones), and 8.3 ± 2.7 C-rich (5.7 ± 2.1 above the TAGB). The excess of O-rich giants is again of a factor of about 6. For the C stars, the 8.3 predicted stars are again inside the 67 % CL of a Poisson distribution of the 6 observed ones. Therefore, also in this case the observed C stars are compatible with the model predictions.

To understand why models using Rizzi's et al. SFH present about half of the C stars as compared to the Dolphin et al. (2005) case, it is instructive to compare the two panels of Fig. 10, the top panel showing the relative SFRs and the bottom one showing the age distribution of different stars for a model galaxy of the same metallicity but with constant SFR. The bottom panel shows that the maximum age for the formation of carbon stars, $t_\mathrm{C}^{\mathrm{max}}$, is close to 6 Gyr ago. This limit is actually determined by the lifetime of the least massive TP-AGB stars in the Marigo & Girardi (2007) models to experience the third dredge up events, with $1.0 \ M_\odot$ (6 Gyr). Below $t_\mathrm{C}^{\mathrm{max}}$ the C stars predominate, above it they are simply absent and the relative number of O-rich TP-AGB stars increases. A substantial fraction of the star formation in Leo II has occurred close to $t_\mathrm{C}^{\mathrm{max}}$, and this determines a marked dependence of the C star counts on the details of the SFR at this age interval. Since the Dolphin et al. (2005) SFR presents a marked episode of star formation between 6 and 8 Gyr, this determines the large number of C stars of the corresponding model.

Were the mass limit for the dredge-up to occur just 10 % (or $0.1 \ M_\odot$) different, $t_\mathrm{C}^{\mathrm{max}}$ would change by as much as ~ 40 %. This would impact very much on the predicted numbers of C-type stars. Also the numbers of O-rich AGB stars would be affected, although somewhat less, since they reflect the complete SFR up to ages of 15 Gyr. The simple fact that the numbers of predicted C-type AGB stars turn out to be consistent with observations within the 95 % CL of a Poisson distribution, would be indicating that *the minimum mass for the formation of C stars at low metallicities is indeed close to 1.0 $M_\odot$*. This is an important indication for the theoretical modeling of AGB stars. We recall that at LMC metallicities, the same mass limit is closer to 1.4 $M_\odot$.
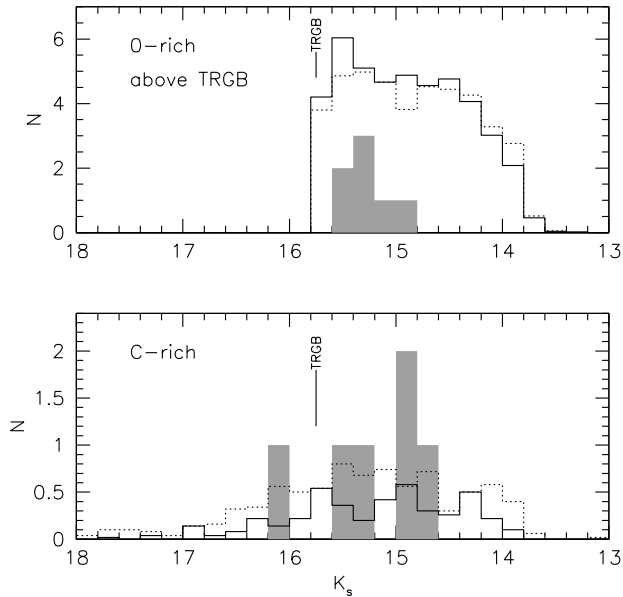
Figure 12. Simulated LFs for luminous stars in Leo II, separated as O-rich giants above $K_s = 15.75$ (*top panel*) and C-rich TP-AGB stars (*bottom panel*), for the Rizzi et al. (in prep.) (*solid line*) and Dolphin et al. (2005, *dotted line*) SFHs. The *grey histograms* correspond to the stars actually observed.

Classical models of stellar evolution[3] have a strong difficulty in reproducing such low mass values for the progenitors of carbon stars (see e.g. Herwig 2005; Stancliffe, Izzard & Tout 2005).

7.4   Luminosity functions

A simple comparison of Fig. 3 and 11 reveals that simulated C stars have about the same K_s magnitudes the observed ones. This is confirmed by the bottom panel of Fig 12 which shows the mean C star luminosity function (as derived from a total of 50 simulations considering the SFR errors) as compared to the data. A KS test indicates a 59 % probability that the observed distribution is drawn by the predicted one, in the case of Rizzi et al. (in prep.) SFR, and a 56 % probability in the case of Dolphin et al. (2005). Also, we note that the presence of a fraction of C stars located below the TRGB is supported by present models.

The top panel of Fig 12 shows the comparison for O-rich giants, limited to the $K_s = 15.75$ interval so as to avoid RGB stars. Here, it is evident that the models predict a distribution extended to brighter magnitudes than observed. The KS probability that the observed distribution is drawn by the predicted one is very low, i.e. lower than 2 % for both Rizzi's et al. and Dolphin et al. (2005) SFRs.

The discrepancy of O-rich giants is statistically significant. The comparison with theoretical isochrones of Fig. 11 suggests that the bright stars missing in the data can be identified either with young early-AGB stars belonging to

populations younger than $\sim$ 3 Gyr, or to the bright section of the TP-AGB for populations older than 7 Gyr. We have verified that eliminating any SFR younger than 4 Gyr from the models, the problem persists. Most of the excess of bright TP-AGB stars is produced by the old populations.

Moreover, the discrepancy in the bright part of the LF is likely related to the excess of O-rich giants that we find in the simulations. In TP-AGB models without third dredge-up, the total lifetime depends essentially on the mass loss efficiency, and particularly on the critical region of the luminosity–temperature plane that triggers a superwind phase where most of the stellar envelope is lost. If the superwind phase is delayed, both the lifetime and the luminosity excursion of the TP-AGB phase would be overestimated. Indeed, anticipating the superwind phase in O-rich models of low mass and metallicity may constitute an interesting solution to the discrepancy we find.

8   SUMMARY AND CONCLUSIONS

We have presented near-infrared JHK_s photometry of a $13\rlap{.}'6 \times 13\rlap{.}'6$ field centred on Leo II dSph, obtained with the new wide field imager WFCAM mounted at the UKIRT telescope. Our data cover most of the extension of Leo II dSph, and are complemented by optical data obtained with the EMMI camera at the ESO NTT telescope.

The good statistics of our database, together with the wide colour baseline, allowed a precise determination of the distance and metallicity of Leo II. We derived a distance modulus $(m - M)_0 = 21.68 \pm 0.11$ from the J, H, and K_s band magnitudes of the TRGB. This is in agreement with optical results, confirming the reliability of our NIR methods.

The $V - K_s$ colours of RGB stars were used to derive the metallicity distribution of the stellar populations of Leo II. Using RGB fiducial lines of GCs as templates, we measured a mean metallicity [M/H] = -1.74. Since the bulk of the stellar population of Leo II is relatively old, we estimated that the population correction to be applied to this value is modest. Assuming a mean age of 9 Gyr yielded a correction of 0.10 dex, from which the age-corrected metallicity is [M/H] = -1.64. Our measurement is in excellent agreement with recent spectroscopic results (Bosler et al. 2007; Koch et al. 2007). A direct comparison between spectroscopic and photometric metallicities of individual stars suggests that the ages derived by Koch et al. (2007) may be underestimated. Indeed, older mean stellar ages would be in better agreement with the SFHs obtained from HST photometry (Hernandez et al. 2000; Dolphin 2002).

We also used our NIR data to define the properties of a nearly complete sample of AGB stars in Leo II dSph. By selecting AGB stars in the NIR two-colour diagram, we were able to discriminate the C-rich from O-rich stellar populations. Foreground Milky Way stars are also easily separated from Leo II AGB members. Our NIR photometry was cross-identified with previous studies of AGB stars, in particular C stars (Azzopardi et al. 1985). One of the 7 carbon star listed by Azzopardi et al. (1985) has anomalous colours, and visual inspection of our images confirms that it is a background galaxy. No indication for additional C stars above the TRGB was found in our analysis, therefore we conclude

---

[3] For classical models we mean models following the Schwarzschild criterion for convective borders, and solving separately for the stellar structure and nucleosynthesis.

that the remaining 6 stars represent the complete population of C stars in Leo II within the area covered by our observations. Using our colour selection, we provide the first sample of O-rich stars in Leo II above the TRGB, with negligible contamination from foreground Milky Way stars.

Our Leo II observations were modeled via simulations based on the HST-derived SFHs, and using the most updated isochrones. The comparison between data and simulations has evidenced both successful and discrepant points, which are all potentially important for the calibration of AGB star models at low metallicity.

With respect to the O-rich TP-AGB stars, the most important discrepancy consists in a predicted over-estimation of their number and mean K_s-band luminosities, as compared to the data. Interestingly, Williams et al. (2007) find similar indications of an excess of AGB stars in the oldest Girardi et al. (2000) isochrones while fitting RGB and AGB stars in the Virgo intracluster stars observed with HST/ACS. A possible solution to this problem could be an increase of mass loss efficiency in O-rich TP-AGB models of low metallicity and low mass. This will be explored in forthcoming work. Regarding this point, we note that:

(i) The obscuration of AGB stars by circumstellar dust could be much more efficient than assumed here for low metallicity, and contribute to the solution of this problem. Indeed, recent Spitzer/IRAC observations of the dwarf irregular galaxies WLM and IC 1613 (Jackson et al. 2007a,b) indicate a very high fraction of optically-obscured AGB stars, of about 40 %. In order to reduce the discrepancies in the LFs for Leo II, dust obscuration should be affecting mainly the O-rich AGB stars of higher luminosities.

(ii) This discrepancy could still be reduced by adopting alternative SFHs. It would be again desirable to have improved derivations of the SFH in dwarf galaxies, based on HST observations covering larger areas than those used by Dolphin et al. (2005) and Rizzi et al. (in prep.). Progress in this sense is expected as the result of ongoing HST surveys and legacy programs on dwarf galaxies (Dolphin et al. 2005; Dalcanton 2006; Gallart 2007).

The above-mentioned discrepancy is still based on too a small sample of observed AGB stars. In forthcoming papers we will extend the comparison to other dwarf galaxies in the Local Group, in order to increase the statistical significance of our conclusions.

With respect to the C-rich TP-AGB stars, the comparison between data and simulations is satisfactory, in terms of location in the colour-magnitude diagram, counts, and luminosity functions. We derive the following important indications:

(i) At low metallicity the minimum mass for a star to become a C star can be as low as $\sim 1\,M_\odot$, which sets an important constraint to the treatment of the third dredge-up in AGB stellar models.

(ii) Low-mass C stars produced by the TP-AGB evolution of single stars (i.e. not belonging to binary systems), are expected to populate the O-rich sequence of giants below the TRGB when they are in the long-lived low-luminosity dips driven by thermal pulses Boothroyd & Sackmann (1988).

(iii) The higher effective temperatures of C stars with bluer $J-K_s$ colours can be a consequence of (a) less efficient molecular formation and opacity at lower metallicity, and/or (b) warming of their Hayashi line during the low-luminosity stages of pulse cycles (see Marigo & Girardi 2007).

From our analysis, we conclude that constraints to the TP-AGB models can be obtained from dwarf galaxies with known SFHs, provided that the numbers of AGB stars are significant and that the SFH is known with sufficient accuracy.

REFERENCES

Aaronson M., Mould J., 1985, ApJ, 290, 191

Aaronson M., Hodge P. W., Olszewski E. W., 1983, ApJ, 267, 271

Aparicio A., Carrera R., Martínez-Delgado D., 2001, AJ, 122, 2524

Albert L., Demers S., Kunkel W. E., 2000, AJ, 119, 2780

Azzopardi M., 2000, in Wing R. F., eds., IAU Symp. 177, Surveys for Carbon Stars in External Galaxies, p. 51

Azzopardi M., Lequeux J., Westerlund B. E., 1985, A&A, 144, 388

Battinelli P., Demers S., 2000, AJ, 120, 1801

Bellazzini M., Gennari N., Ferraro F. R., 2005, MNRAS, 360, 185

Bessell M. S., Brett J. M., 1988, PASP, 100, 1134

Blum R. D., et al., 2006, AJ, 132, 2034

Bolatto A. D., Simon J. D., Stanimirović S., van Loon J. T., Shah R. Y., Venn K., Leroy A. K., Sandstrom K., Jackson J. M., Israel F. P., Li A., Staveley-Smith L., Bot C., Boulanger F., Rubio M., 2007, ApJ, 655, 212

Bonatto C., Bica E., Girardi L., 2004, A&A, 415, 571

Boothroyd A. I., Sackmann I.-J., 1988, ApJ, 328, 632

Bosler T. L., Smecker-Hane T. A., Stetson P. B., 2007, MNRAS, 378, 318

Calabretta M. R., Greisen E. W., 2002, A&A, 395, 1077

Carretta E., Gratton R. G., 1997, A&AS, 121, 95

Cioni M. R., Habing H. J., Loup C., Groenewegen M. A. T., Epchtein N., Consortium T. D., 1999, in Whitelock P., Cannon R., eds, IAU Symp. 192, The Stellar Content of Local Group Galaxies, 65

Cioni M.-R. L., et al., 2003, A&A, 406, 51

Coleman M. G., Jordi K., Rix H.-W., Grebel E. K., Koch A., 2007, AJ, 134, 1938

Da Costa G. S., Armandroff T. E., 1990, AJ, 100, 162

Dalcanton J., 2006, in American Astronomical Society Meeting Abstracts Vol. 209, The ACS Nearby Galaxy Survey Treasury: Overview, p. 114

Dolphin A. E., 2002, MNRAS, 332, 91

Dolphin A. E., Weisz D. R., Skillman E. D., Holtzman J. A., 2005, (arXiv:astro-ph/0506430)

Dye S., et al., 2006, MNRAS, 372, 1227

Ferraro F. R., Paltrinieri B., Rood R. T., Dorman B., 1999, ApJ, 522, 983

Gallart C., The LCID Team, 2007, in IAU Symposium 241: "Stellar Populations as Building Blocks of Galaxies", p.290

Gallart C., Aparicio A., Vilchez J. M., 1996, AJ, 112, 1928

Geisler D., Wallerstein G., Smith V. V., Casetti-Dinescu D. I., 2007, PASP, 119, 939

Girardi L., Marigo P., 2007, in Kerschbaum F., Charbonnel C., Wing R. F., eds., ASP Conf. Ser. 378, Why Galaxies Care About AGB Stars: Their Importance as Actors and Probes. ASP, San Francisco, p.20

Girardi L., Bressan A., Bertelli G., Chiosi C., 2000, A&AS, 141, 371

Girardi L., Bertelli G., Bressan A., Chiosi C., Groenewegen M. A. T., Marigo P., Salasnich B., Weiss A., 2002, A&A, 391, 195

Girardi L., Groenewegen M. A. T., Hatziminaoglou E., da Costa L., 2005, A&A, 436, 895

Gullieuszik M., Held E. V., Rizzi L., Saviane I., Momany Y., Ortolani S., 2007a, A&A, 467, 1025

Gullieuszik M., Rejkuba M., Cioni M. R., Habing H. J., Held E. V., 2007b, A&A, 475, 467

Groenewegen M. A. T., 2006, A&A, 448, 181

Groenewegen M. A. T., et al., 2002, A&A, 392, 741

Hernandez X., Gilmore G., Valls-Gabaud D., 2000, MNRAS, 317, 831

Herwig F., 2005, ARA&A, 43, 435

Jackson D. C., Skillman E. D., Gehrz R. D., Polomski E., Woodward C. E., 2007a, ApJ, 667, 891

Jackson D. C., Skillman E. D., Gehrz R. D., Polomski E., Woodward C. E., 2007b, ApJ, 656, 818

Komiyama Y., et al., 2007, AJ, 134, 835

Koch A., Grebel E. K., Kleyna J. T., Wilkinson M. I., Harbeck D. R., Gilmore G. F., Wyse R. F. G., Evans N. W., 2007, AJ, 133, 270

Lee M. G., 1995, AJ, 110, 1155

Lee M. G., Freedman W. L., Madore B. F., 1993, ApJ, 417, 553

Loidl R., Lançon A., Jørgensen U. G., 2001, A&A, 371, 1065

Makarov D., Makarova L., Rizzi L., Tully R. B., Dolphin A. E., Sakai S., Shaya E. J., 2006, AJ, 132, 2729

Mapelli M., Ripamonti E., Tolstoy E., Sigurdsson S., Irwin M. J., Battaglia G., 2007, MNRAS, 380, 1127

Marigo P., Girardi L., 2007, A&A, 469, 239

Marigo P., Girardi L., Bressan A., Groenewegen M. A. T., Silva L., Granato G. L., 2008, A&A, in press (arXiv:0711.4922)

Mighell K. J., Rich R. M., 1996, AJ, 111, 777

Momany Y., Held E. V., Saviane I., Rizzi L., 2002, A&A, 384, 393

Momany Y., Held E. V., Saviane I., Zaggia S., Rizzi L., Gullieuszik M., 2007, A&A, 468, 973

Nikolaev S., Weinberg M. D., 2000, ApJ, 542, 804

Nowotny W., Kerschbaum F., Schwarz H. E., Olofsson H., 2001, A&A, 367, 557

Rieke G. H., Lebofsky M. J., 1985, ApJ, 288, 618

Rizzi L., Held E. V., Saviane I., Tully R. B., Gullieuszik M., 2007, MNRAS, 380, 1255

Salaris M., Girardi L., 2005, MNRAS, 357, 669

Saviane I., Rosenberg A., Piotto G., Aparicio A., 2000, A&A, 355, 966

Skrutskie M. F., et al., 2006, AJ, 131, 1163

Stancliffe R. J., Izzard R. G., Tout C. A., 2005, MNRAS, 356, L1

Stetson P. B., 1987, PASP, 99, 191

Stetson P. B., 1994, PASP, 106, 250

Totten E. J., Irwin M. J., Whitelock P. A., 2000, MNRAS, 314, 630

Valenti E., Ferraro F. R., Origlia L., 2004a, MNRAS, 351, 1204

Valenti E., Ferraro F. R., Origlia L., 2004b, MNRAS, 354, 815

Williams B. F., Ciardullo R., Durrell P. R., Vinciguerra M., Feldmeier J. J., Jacoby G. H., Sigurdsson S., von Hippel T., Ferguson H. C., Tanvir N. R., Arnaboldi M., Gerhard O., Aguerri J. A. L., Freeman K., 2007, ApJ, 656, 756

Whitelock P. A., Feast M. W., Marang F., Groenewegen M. A. T., 2006, MNRAS, 369, 751